

ARTICLE

Molecular Complementarity and Structural Heterogeneity within Co-assembled Peptide β -Sheet Nanofibers

Kong M. Wong,^a Yiming Wang,^b Dillon T. Seroski,^c Grant E. Larkin,^a Anil K. Mehta,^d Gregory A. Hudalla,^c Carol K. Hall,^b and Anant K. Paravastu^{*a}

Received 00th January 20xx,
Accepted 00th January 20xx

DOI: 10.1039/x0xx00000x

Self-assembling peptides have garnered an increasing amount of interest as a functional biomaterial for medical and biotechnological applications. Recently, β -sheet peptide designs utilizing complementary pairs of peptides composed of charged amino acids positioned to impart co-assembly behavior have expanded the portfolio of peptide aggregate structures. Structural characterization of these charge-complementary peptide co-assemblies has been limited. Thus, it is not known how the complementary peptides organize on the molecular level. Through a combination of solid-state NMR measurements and discontinuous molecular dynamics simulations, we investigate the molecular organization of King-Webb peptide nanofibers. KW+ and KW- peptides co-assemble into near stoichiometric two-component β -sheet structures as observed by computational simulations and ^{13}C - ^{13}C dipolar couplings. A majority of β -strands are aligned with antiparallel nearest neighbors within the β -sheet as previously suggested by Fourier transform infrared spectroscopy measurements. Surprisingly, however, a significant proportion of β -strand neighbors are parallel. While charge-complementary peptides were previously assumed to organize in an ideal $(\text{AB})_n$ pattern, dipolar recoupling measurements on isotopically diluted nanofiber samples reveal a non-negligible amount of self-associated (AA and BB) pairs. Furthermore, computational simulations predict these different structures can coexist within the same nanofiber. Our results highlight structural disorder at the molecular level in a charge-complementary peptide system with implications on co-assembling peptide designs.

Introduction

The design of self-assembling peptide sequences has advanced our fundamental understanding of sequence-to-structure relationships governing supramolecular peptide architectures. One commonly desired nanostructure includes peptide nanofibers that often form physically entangled network gels that are biocompatible and capable of various functionalization chemistries.¹ These properties make them well-suited for a range of biotechnological applications including tissue engineering,^{2, 3} drug delivery,^{4, 5} and immunotherapy.⁶⁻⁸ Co-assembling β -sheet peptides are beginning to be designed and synthesized.⁹⁻¹⁴ Thereby expanding the number of known supramolecular architectures and our ability to immobilize biomolecules on peptide nanofiber surfaces. While hundreds of self-assembling β -sheet peptides have been identified,¹⁵⁻¹⁸ only a few designer co-assembling β -sheet pairs are known,^{9-14, 19} with no naturally-occurring examples. In principle, a vast array

of designer co-assembling β -sheet peptides are possible. However, little is understood with regard to the interactions that promote complementary β -sheet co-assembly, and structural analysis of existing co-assembling β -sheet designs has been limited.

Current co-assembling peptide designs rely on complementary interactions between charged variants of known self-assembling peptides. An early example of complementary electrostatic sequences comes from Pandya et al. with the SAF-p1 and SAF-p2 peptides which form heteromeric coiled-coil peptide nanofibers via association of the “sticky-ends.”²⁰ P₁₁-4 and P₁₁-5, one of the first co-assembling β -sheet-forming pairs, were designed based off the self-assembling peptide DN1 created by Aggeli and coworkers to have opposing isoelectric points that prevented their self-association at neutral pH.^{14, 21} Mixtures of the P₁₁-4 and P₁₁-5 peptides readily formed β -sheet rich nanofibers as observed by Fourier Transform Infrared (FT-IR) and circular dichroism (CD) spectroscopy.¹⁴ Seroski et al. developed charged variants of the self-assembling Q11 peptide that resist self-assembly but promote co-assembly as assessed by CD and ThT fluorescence measurements.^{10, 22} Charged variants of A β (16-22) have been shown by Li et al. to mix and assemble into double-layered nanotubes with the negatively charged peptide surrounding the positively charged inner layer of the peptide nanotube.¹⁹ Other iterations utilizing this design principle of charge complementarity led to the P₁₁-14 and P₁₁-13 peptides by Kyle et al. and the p1 and p2 peptides by King, Webb, and

^a School of Chemical and Biomolecular Engineering, Georgia Institute of Technology, Atlanta, GA 30332, United States

^b Department of Chemical and Biomolecular Engineering, North Carolina State University, Raleigh, NC 27695-7905, United States

^c J. Crayton Pruitt Family Department of Biomedical Engineering, University of Florida, 1275 Center Drive, Biomedical Sciences J293, P.O. BOX 116131, Gainesville, FL 32611, United States

^d National Magnetic Resonance Lab and McKnight Brain Institute, University of Florida, Box 10015, Gainesville, FL, 32610, United States

Electronic Supplementary Information (ESI) available: [details of any supplementary information available should be included here]. See DOI: 10.1039/x0xx00000x

coworkers.^{11, 13} The latter is the focus of our study which we herein refer to as the King-Webb peptides, comprised of KW+ (KKFEWFEKK) and KW- (EEFKWKFKKE).

Prior structural characterization of co-assembled KW+ and KW- peptide nanofibers by attenuated total reflectance FT-IR spectroscopy suggests a co-assembled antiparallel β -sheet structure.¹¹ While a lower amide I' maxima and presence of a low-intensity peak around 1685 cm^{-1} in FT-IR spectra has often been attributed to antiparallel β -sheets, several experimental and theoretical studies have argued that this interpretation is not always true.²³ Our own work on RADA16-I revealed a parallel β -sheet structure with a 2-residue registry shift contradicting the proposed antiparallel β -sheet model.^{24, 25} Included in this classification of a co-assembled antiparallel β -sheet structure are three assumptions. First, KW+ and KW- peptides interact at the molecular level to form two-component nanofibers rather than self-sorting. Second, KW+ and KW- peptides arrange in a perfect alternation within a β -sheet. Third, nanofibers contain equal amounts of KW+ and KW- peptides. Currently, there is no direct biophysical evidence to support these assumptions and resolve these structural details.

In this study, we assess the co-assembled antiparallel β -sheet structural model and test the assumptions in the King-Webb peptide system through a combination of computer simulations, solid-state nuclear magnetic resonance (NMR) experiments and biophysical measurements. Coarse-grained

discontinuous molecular dynamics (DMD) simulations of 48 KW+ and 48 KW- chains accurately predict co-assembly behavior, and NMR results support molecular-level interactions between peptide components as expected in co-assembled nanofibers. Although the experimental and computational results indicate some preference for antiparallel β -sheet structure and alternation of complementary β -strands, a high percentage (31.7%) of β -strands are oriented parallel to at least one nearest neighbor with a significant amount of peptide self-association. The structural heterogeneity in the co-assembled KW+ and KW- peptide nanofibers, which appears to occur within each co-assembled peptide nanofiber, stands in contrast to typical behavior seen in self-assembling β -sheet peptides. In self-assembled peptide nanofibers, structure may vary between nanofibers in the same sample, but is believed to be consistent within individual nanofibers.²⁶⁻²⁹

Results

King-Webb Peptides Exhibit Molecular-Level Co-Assembly into β -Sheet Rich Nanofibers.

Complementary interactions between KW+ and KW- peptides drive assembly into long β -sheet rich nanofibers. Figure 1a shows a TEM image of a negatively-stained nanofiber sample formed from an equimolar mixture of KW+ and KW- peptides at

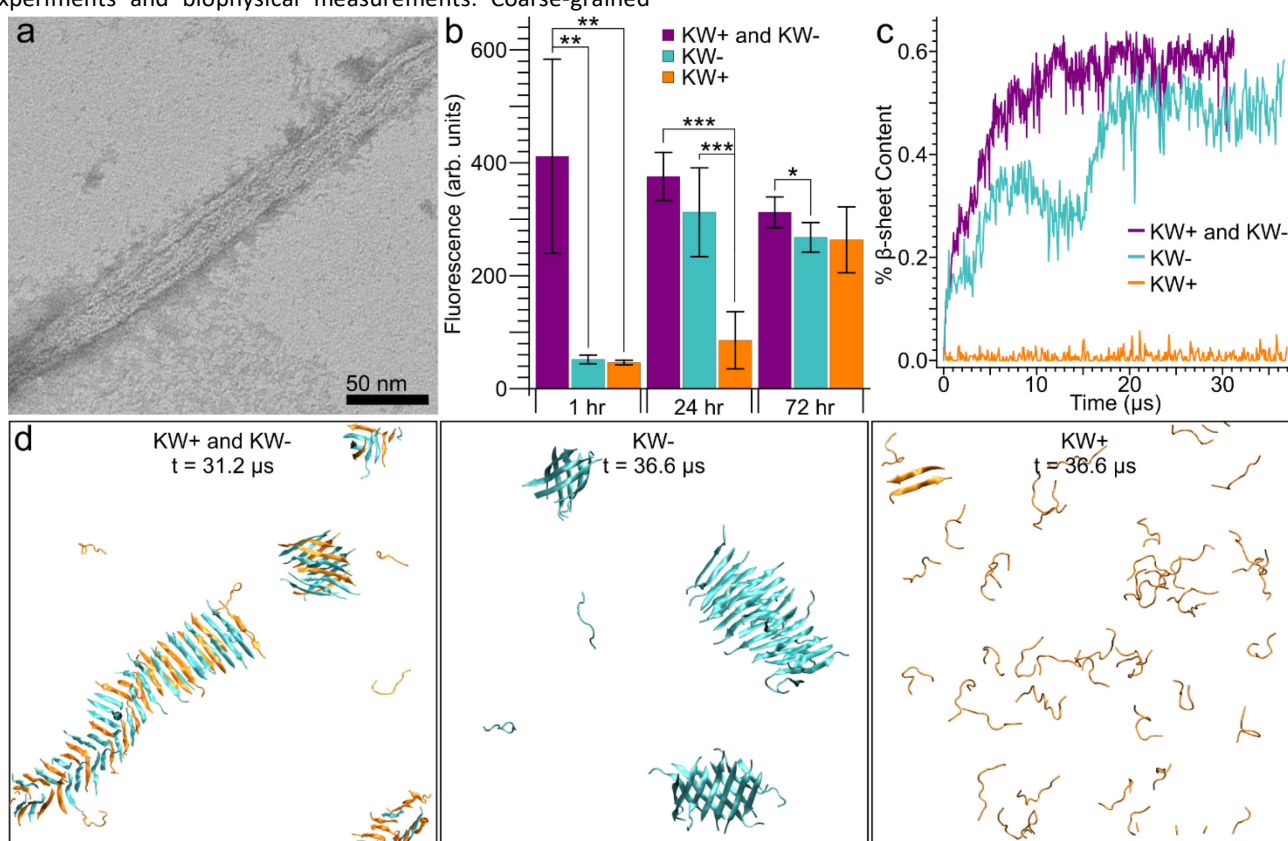


Figure 1. Complementary interactions are kinetically favored in KW co-assembly. a) TEM image of a negatively-stained KW peptide nanofiber bundle. b) ThT fluorescence measurements of peptide solutions containing KW+ only, KW- only, and an equimolar mixture of KW+ and KW- at different assembly times. Error bars signify 95% confidence intervals, * $p \leq 0.05$, ** $p \leq 0.01$, *** $p \leq 0.001$ by Student's t-test. c) Percentage of β -sheet content over simulation time for 48 KW+ chains (orange), 48 KW- chains (cyan), and a mixture of 48 KW+ and 48 KW- chains (purple). d) Simulation snapshots of β -sheet nanofibers composed of KW+ strands (orange) and/or KW- strands (cyan) at specified times.

10mM concentration in 10X PBS. Fibers span microns in length and striations are visible indicating fiber bundling consistent with previous observations by the peptide designers.¹¹ Thioflavin T (ThT) fluorescence measurements of KW+, KW-, and an equimolar mixture of KW+/KW- shown in Figure 1b suggest complementary interactions are kinetically favored during assembly. ThT demonstrates enhanced fluorescence emission (Figure 1b) upon binding to β -sheet rich peptide nanofibers and increasing fluorescence corresponds to an increase in peptide nanofibers.^{30,31} Individual aqueous solutions of KW+ and KW- peptides in 10X PBS show little fluorescence at 1 hour while the equimolar mixture of KW+ and KW- shows a higher fluorescence intensity indicating assembly. The formation of β -sheet rich nanofibers in KW+ and KW- mixtures as shown by ThT fluorescence agrees with prior FT-IR measurements by King et al.¹¹ Fluorescence of KW+ and KW- single-peptide solutions increases over a few days indicating self-assembly over time. King et al. previously observed the formation of weak gels after several hours indicative of self-assembly at room temperature.¹¹ In addition, the KW- peptide exhibits a higher propensity for self-assembly than the KW+ peptide. This observation agrees with prior FT-IR measurements by King et al. on single-peptide solutions of KW- and KW+ in 50 mM NaCl in which the formation of β -sheets was only observed in the KW- solution after 20 minutes of incubation.¹¹ Coarse-grained DMD simulations of 48 KW+ or 48 KW- chains (Figure 1c-d and Figure S1 in Supporting Information) were performed to evaluate the propensity for self-assembly in silico. Formation of β -barrel-like oligomers and β -sheet nanofibers during simulation is observed in Figure 1d and Figure S1. Remarkably, computational simulations qualitatively agree with the observation that the KW- peptide is more prone to self-assembly than the KW+ peptide, which remains as weakly associating random coils in simulations. Simulations of mixtures of 48 KW+ and 48 KW- chains are also consistent with the experimental observation that the mixture assembles more quickly than either of the pure peptides (Figure 1c).

Solid-state NMR and computational results for equimolar mixtures of King-Webb peptides provide direct molecular-level evidence of a co-assembled nanofiber structure. To confirm this model, nearest-neighbor proximities between KW+ and KW- peptides were measured by 2-dimensional (2D) solid-state NMR. Nanofiber samples were prepared with uniform ^{13}C and ^{15}N isotopic enrichment at residue positions F3 and K9 on KW+ and E1 on KW- (Sample A). Table 1 lists samples investigated in this study with different residues isotopically labeled for NMR measurements. In Figure 2, 2D Dipolar Assisted Rotational Resonance (DARR) spectra of centrifuged and lyophilized nanofiber samples show measurable intermolecular contacts (off-diagonal “crosspeaks” between atoms on different residues) between KW+ and KW- peptides,³² supporting co-assembly at the molecular level. Solid colored lines in Figure 2 illustrate NMR peak assignments for the ^{13}C isotopically enriched amino acids determined from analysis of 1-bond correlations in the finite-pulse radio-frequency driven recoupling (fpRFDR) NMR spectra shown in Figure S3.^{33, 34} Contacts between E1 and K9 as well as E1 and F3, marked by

Table 1. Isotopic labeling schemes for co-assembled KW fibril samples

Sample	KW+ peptide	KW- peptide
A	U^{13}C and U^{15}N on F3 and K9	U^{13}C and U^{15}N on E1
B	U^{13}C and U^{15}N on F3 and K9	unlabeled
C	unlabeled	U^{13}C and U^{15}N on E1
D	unlabeled	unlabeled
E	^{13}C on CO of F3 and ^{15}N on K9	^{13}C on CO of F3
F	^{13}C on CO of F3 and ^{15}N on K9	unlabeled
G	unlabeled	^{13}C on CO of F3

*All nanofibers samples prepared under that same standard hydrogel preparation as noted in methods section.

** U denotes uniform ^{13}C or ^{15}N enrichment of specified amino acid.

red-blue and red-green bi-color circles, indicate inter-residue distances (distances between the closest pair of ^{13}C atoms on different residues) up to 0.6 nm between the specified amino acids. 1D slices of the DARR spectra are included in Figure S2. Similarly, examination of the nanofibers in Figure 1d from a coarse-grained DMD simulation of a mixture of 48 KW+ (orange) and 48 KW- (cyan) chains shows mixing within resulting assemblies indicative of a co-assembled structure.

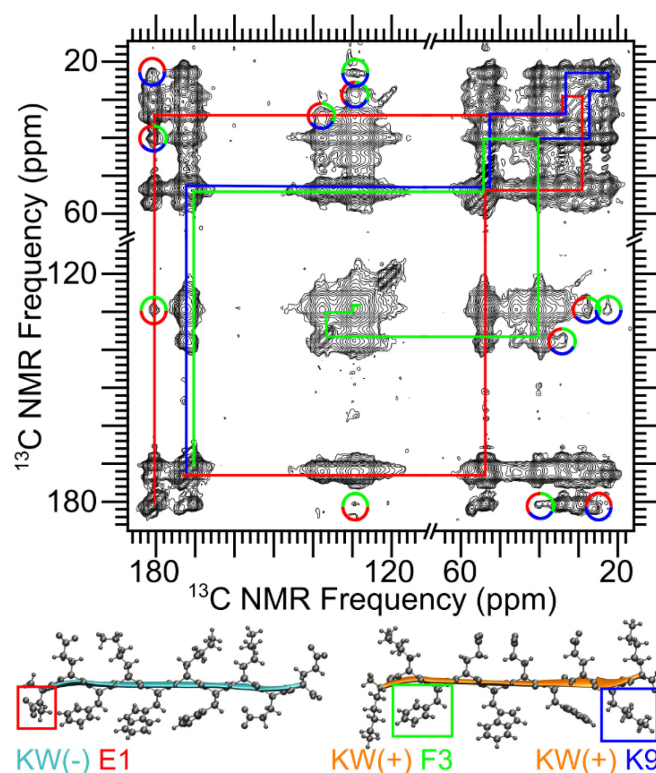


Figure 2. Molecular-level evidence of King-Webb peptide co-assembly. 2D ^{13}C - ^{13}C 500ms DARR spectrum of an isotopically enriched KW peptide nanofiber sample (Sample A). Colored lines indicate spectral assignments for isotopically enriched residues determined by 2D fpRFDR. Bi-colored circles highlight off-diagonal crosspeaks resulting from inter-residue ^{13}C - ^{13}C couplings. Tri-colored circles indicate overlapping crosspeaks with signal contributions from 3 residues.

The co-assembled nanofibers are composed of near stoichiometric amounts of KW+ and KW- peptides. Though equimolar solutions of the complementary peptides are mixed together to initiate assembly, it has not been previously shown whether the peptides are present in equal abundance within the final structure. To evaluate the relative amounts of each peptide incorporated into the co-assembled nanofibers, a ^{13}C NMR spectrum was collected for Sample A using a method developed by Duan et. al. to produce a spectrum in which NMR peak intensities quantitatively represent relative numbers of underlying ^{13}C sites.³⁵ In Figure 3a, peak positions (chemical shifts) uniquely attributable to the carboxyl carbon ($\text{C}\delta$) on glutamic acid and the γ -carbon ($\text{C}\gamma$) on lysine sidechains are highlighted in red and blue, respectively.³⁶⁻³⁸ The ratio of the peak areas ($\text{KW}^+ \text{K9 C}\gamma$ to $\text{KW}^- \text{E1 C}\delta$) was 1.12 ± 0.03 to 1. The

presence of both peptide components at a near stoichiometric ratio further supports complementary interactions as a contributing factor in the co-assembly of KW peptides.

The NMR spectra show evidence of structural heterogeneity. The behavior is most clearly observed in NMR peak splitting, where more than one NMR peak is observed for individual isotopically enriched sites (Figure 3). Chemical shifts are sensitive to the local electronic environment surrounding ^{13}C sites (bond angles, arrangement of nearest-neighbor atoms) and differences in peptide nanofiber structure can result in distinct environments that produce different chemical shifts.^{26, 27, 39} Figure 3b exhibits this behavior in ^{15}N chemical shifts, where 2D ^{13}C - ^{15}N Transferred-Echo Double-Resonance (TEDOR) measurements were performed on Samples A, B, and C.⁴⁰ 2D

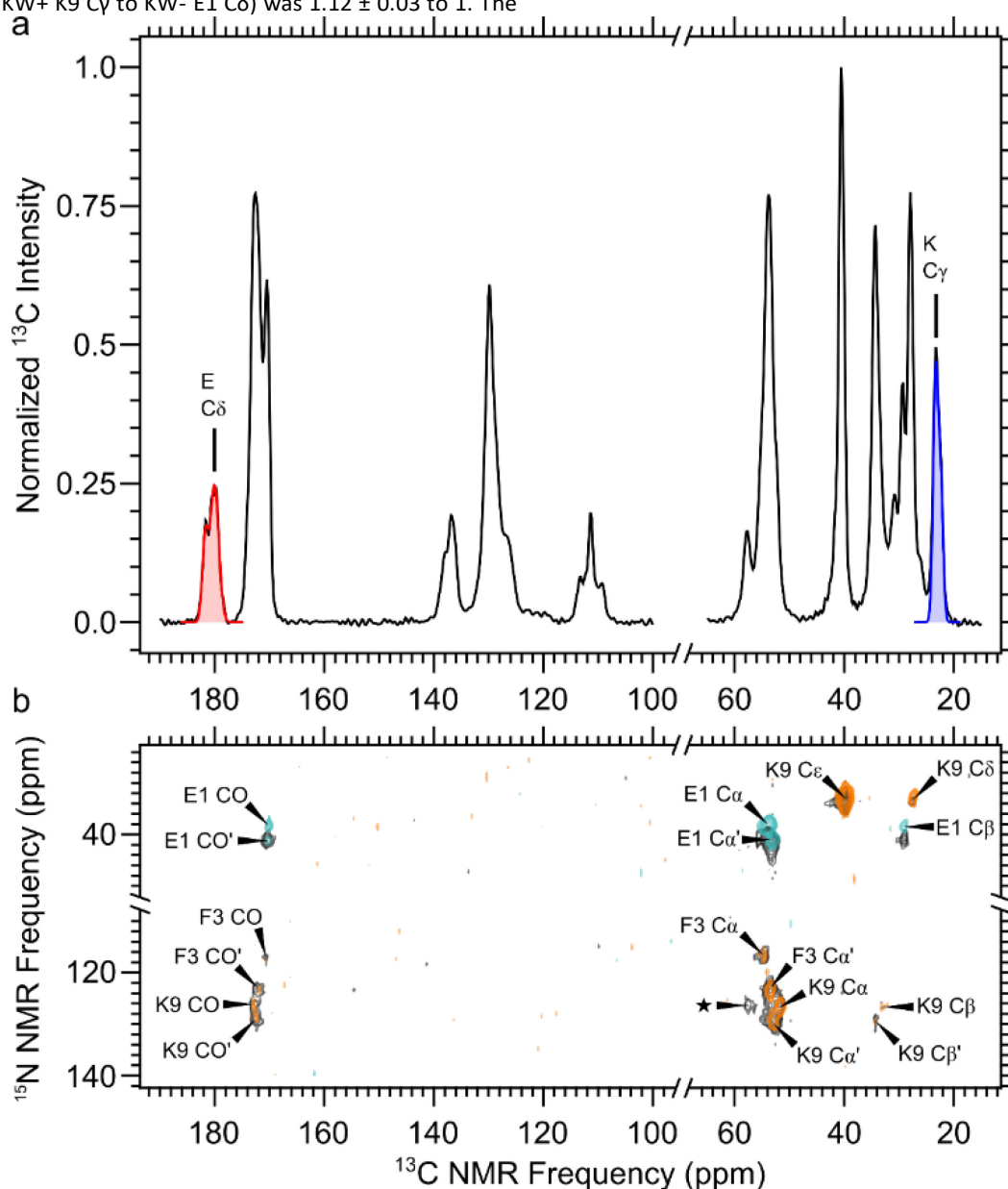


Figure 3. KW+ and KW- peptide co-assembly stoichiometrically into β -sheet nanofibers. a) A quantitative ^{13}C spectrum of Sample A, which was isotopically labeled at E1 on KW- and F3 and K9 on KW+. Chemical shifts unique to KW+ and KW- are highlighted in blue and red, respectively. b) An overlay of 2D ^{13}C - ^{15}N TEDOR spectra of Samples A, B, and C, corresponding to black, cyan, and orange contours, respectively. All three spectra were collected with 2.4 ms of ^{13}C - ^{15}N mixing time. Chemical shift assignments indicated by arrows were determined by comparison with a 2D fpRFDR spectrum. Multiple assignments resulting from peak splitting are distinguished by an apostrophe (').

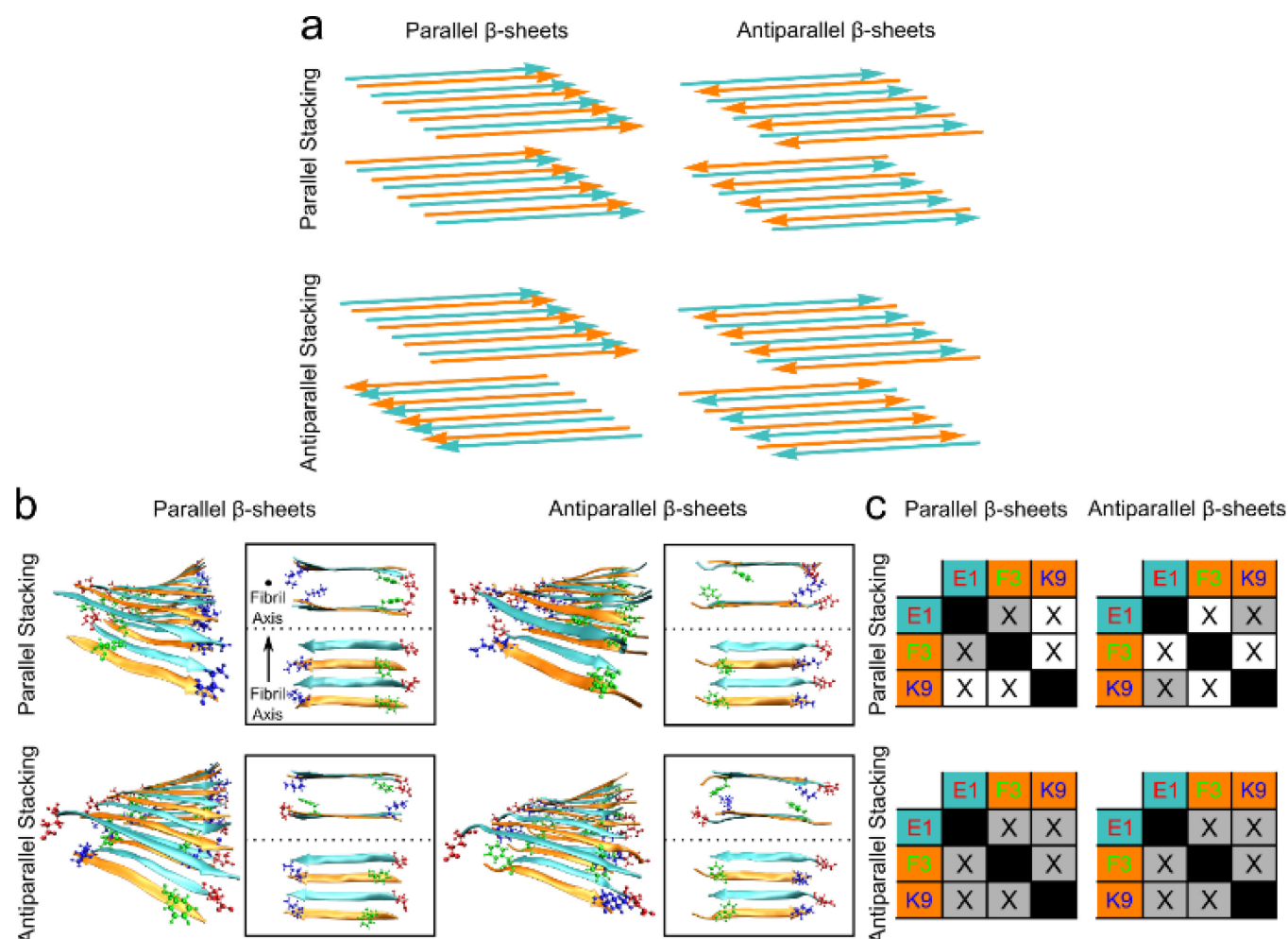


Figure 4. Multiple co-assembled structures are possible as suggested by comparing experimental NMR results against predicted intermolecular contacts. a) Cartoon illustrations of 4 ideal co-assembled β -sheet configurations considered. Colored arrows pointing from N-terminal to C-terminal represent KW+ (orange) and KW- (cyan). b) Images of all-atom molecular models for the 4 idealized co-assembled β -sheet structures are shown. Cross-sectional and single sheet views are included to show predicted intermolecular contacts. c) Intermolecular contact tables based on the labeling scheme shown in part b. Gray squares depict computationally predicted intermolecular contacts. The symbol X marks experimentally observed intermolecular contacts from NMR measurements on labeled samples.

TEDOR peaks arise because of magnetization transfer between $^{13}\text{C}/^{15}\text{N}$ that experience distance-dependent dipolar couplings.⁴⁰ Multiple spectral assignments were made for each of the enriched amino acids providing further evidence for structural heterogeneity in the co-assembled King-Webb peptide nanofibers. As shown in Figure 3b, two peaks are observed for some near-backbone carbons and nitrogens suggesting at least 2 distinct chemical environments or structures exist. The starred NMR peak matches the peak position of a lysine α -carbon in a random coil configuration possibly indicating unassembled material in the sample.³⁶⁻³⁸ However, other random coil signatures such as a lysine carbonyl carbon peak around 176.5ppm are not observed. Analysis of NMR peak linewidths in a ^{13}C NMR spectrum (Figure S4) of a naturally abundant nanofiber sample, Sample D, indicate broad linewidths (~ 2.5 ppm). These broad linewidths are 5 times wider than those observed in protein crystals (0.5-0.6 ppm),⁴¹ and while many factors contribute to line broadening, these linewidths are consistent with the presence of multiple local environments that would be expected from nanofibers having structural heterogeneity as indicated by the simulations.

Antiparallel and Parallel β -Sheets Are Detected in King-Webb Peptide Nanofibers.

Four distinct β -strand arrangements in co-assembled peptide nanofibers were considered and compared using constrained 3D models of each arrangement. In Figure 4a, the 4 cross β -sheet structures considered consist of either parallel or antiparallel β -sheets that are stacked parallel or antiparallel to one another.⁴² Each structure assumes a hydrophobic core such that the hydrophobic face of each peptide is shielded from water. In addition, each peptide component is assumed to be surrounded only by complementary peptides as nearest neighbors. We note that, when self-assembled antiparallel β -sheets stack, structures generated from different orientations of the individual sheets are typically indistinguishable. However, in the case of co-assembling peptide β -sheets, the relative orientation of each peptide component between the two β -sheets is unique for antiparallel and parallel stacking leading to distinct arrangements; examine, for example, only the orange arrows for antiparallel β -sheets, stacked parallel and antiparallel, in Figure 4a. Figure 4b shows all-atom molecular models created from constrained MD simulations of 10 KW-

peptides and 10 KW+ peptides arranged according to the cartoon illustrations in Figure 4a. Dihedral angles and hydrogen bonds were constrained according to expected angles and bond lengths for a cross- β nanofiber.

Comparison of observed 2D DARR contacts with those predicted from aforementioned molecular models suggest that the β -sheets stack antiparallel to one another. In Figure 4b, amino acid sidechains are drawn that correspond to the isotopically-enriched amino acids in Sample A. Cross-sectional and single β -sheet views highlight the relative orientation of isotopically-enriched amino acids. Each structural arrangement produces a different set of predicted intermolecular contacts (gray squares) summarized in the DARR contact tables displayed in Figure 4c. NMR results indicate that all 3 intermolecular contacts (marked as 'X' in DARR contact tables) are observed. The presence of a contact between F3 and K9 labeled on the same peptide suggests that antiparallel stacking of the β -sheets occurs. Though antiparallel stacking must exist in the sample, observation of all 3 contacts does not rule out the existence of parallel stacked structures also existing because of the predicted parallel contacts are a subset of the antiparallel contacts. Thus, while the 2D DARR results provide some insight into the stacking in the nanofiber, more quantitative measurements are needed to discern between parallel and antiparallel β -sheet structures.

Dipolar recoupling NMR measurements suggest a preference toward antiparallel β -sheets, but surprisingly, a significant fraction of parallel β -sheets are present (Figure 5). By ^{13}C isotopically enriching only the carbonyl (CO) of F3 on KW+ and KW- peptides as shown in Figure 5a, we can measure distance-dependent ^{13}C - ^{13}C dipolar couplings with PITHIRDS-CT to assess parallel β -sheet content in co-assembled nanofiber samples.⁴³ In a parallel β -sheet, the ^{13}C - ^{13}C interstrand spacing is expected to be 0.5 nm giving rise to a strong dipolar coupling and a strong ^{13}C signal decay in the PITHIRDS-CT experiment (Black solid line in Figure 5c). On the other hand, an antiparallel β -sheet structure increases the ^{13}C - ^{13}C spacing to 1.0 nm leading to a weak dipolar coupling and a small decay in ^{13}C signal (Green solid line in Figure 5c). Results of PITHIRDS-CT experiments on Sample E suggest a mixture of strongly and weakly coupled spins. In Figure 5c, measurements of ^{13}C signal (black dots) rapidly decay at early recoupling times before flattening out. Fitting by a linear combination of the solid green and black decays maps to 53.4% of the full signal decay. Therefore, the parallel β -sheet content is calculated to be 31.7% assuming each coupling is an independent event. In the same sample, KW+ peptides were isotopically enriched with ^{15}N at K9 to independently evaluate ^{15}N - ^{13}C dipolar couplings. As demonstrated in Figure 5b, an antiparallel β -sheet arrangement results in a 0.5 nm ^{15}N - ^{13}C interstrand spacing, creating a strong heteronuclear coupling. Consequently, a weak coupling is expected in the parallel β -sheet case. The $^{13}\text{C}\{^{15}\text{N}\}$ REDOR experiment measures ^{13}C - ^{15}N dipolar couplings, hence ^{13}C - ^{15}N interstrand spacing.^{44, 45} A ^{15}N - ^{13}C distance of 0.5 nm is shown by the solid black curve in Figure 5d and generates a strong ^{13}C - ^{15}N dipolar coupling. However, a ^{15}N - ^{13}C distance of 1.0 nm has a weaker dipolar coupling resulting in a significantly smaller

REDOR dephasing as depicted in Figure 5d as a solid green curve. Supporting the theory of a heterogeneous β -sheet structure, antiparallel β -sheet content is estimated to be between 56.4% and 62.2% from $^{13}\text{C}\{^{15}\text{N}\}$ REDOR measurements on Sample E. While both antiparallel and parallel β -sheets are detected, it is unclear whether the two structures exist in the same nanofiber or self-sort into ideal parallel β -sheets and ideal antiparallel β -sheets.

Analysis of coarse-grained DMD simulations corroborates experimental observations of structural heterogeneity and unveils a possible minority population of out-of-register antiparallel β -sheets. Intermolecular distances between F3 CO sites on both KW+ and KW- peptides were examined in the final frames of the DMD simulations mimicking the experimental design of our PITHIRDS-CT measurements. In Figure S5, we plot the relative distribution of F3 CO to F3 CO interstrand distances averaged over 6 simulation runs. In an ideal parallel β -sheet structure, a prominent peak would appear at 0.5 nm, whereas an antiparallel β -sheet would only show a peak at 1.0 nm or longer. The interstrand distance distribution between F3 CO sites shows a peak at 0.5 nm consistent with PITHIRDS-CT results indicating a measureable amount of parallel β -sheet structure. Calculation of the predicted parallel β -sheet content suggests 40.2% of KW peptides are oriented parallel which is higher than estimated from PITHIRDS-CT measurements. Similarly, analysis of the interstrand distance distribution between the F3 CO on KW- and K9 backbone N on KW+ qualitatively agrees with experimental REDOR results that predict antiparallel β -sheet content in the co-assembled nanofiber. Simulations predict 54.0% antiparallel β -sheet content which is comparable to the experimentally measured value. Table 2 summarizes the computationally predicted and experimentally observed β -sheet structure content. Figure 5e shows a sample co-assembled King-Webb nanofiber observed at the end of a DMD simulation. Computational simulations predict a preference for the antiparallel orientation in agreement with the experimental results. Surprisingly, DMD simulations reveal the presence of out-of-register antiparallel β -sheets, which result in molecules that are not oriented perfectly perpendicular to the nanofiber axis (see Figure 5e). This feature is also exhibited in Figure S5, with the peak near 0.8 nm. A small population of out-of-register antiparallel β -sheets could be consistent with the behavior observed at longer recoupling times in the PITHIRDS-CT and REDOR measurements: simulations predict plateaus in NMR intensity, which are not observed in the data. Lastly, the simulations predict that in-register parallel, in-register antiparallel, and out-of-register antiparallel β -sheets can coexist in the same nanofiber rather than self-sorting into structurally distinct fibers.

Table 2. Comparison of predicted and experimentally measured parallel and antiparallel β -sheet content

	DMD Simulations	NMR Measurements
Parallel β -sheets	40.2%	31.7%
Antiparallel β -sheets	54.0%	56.4%

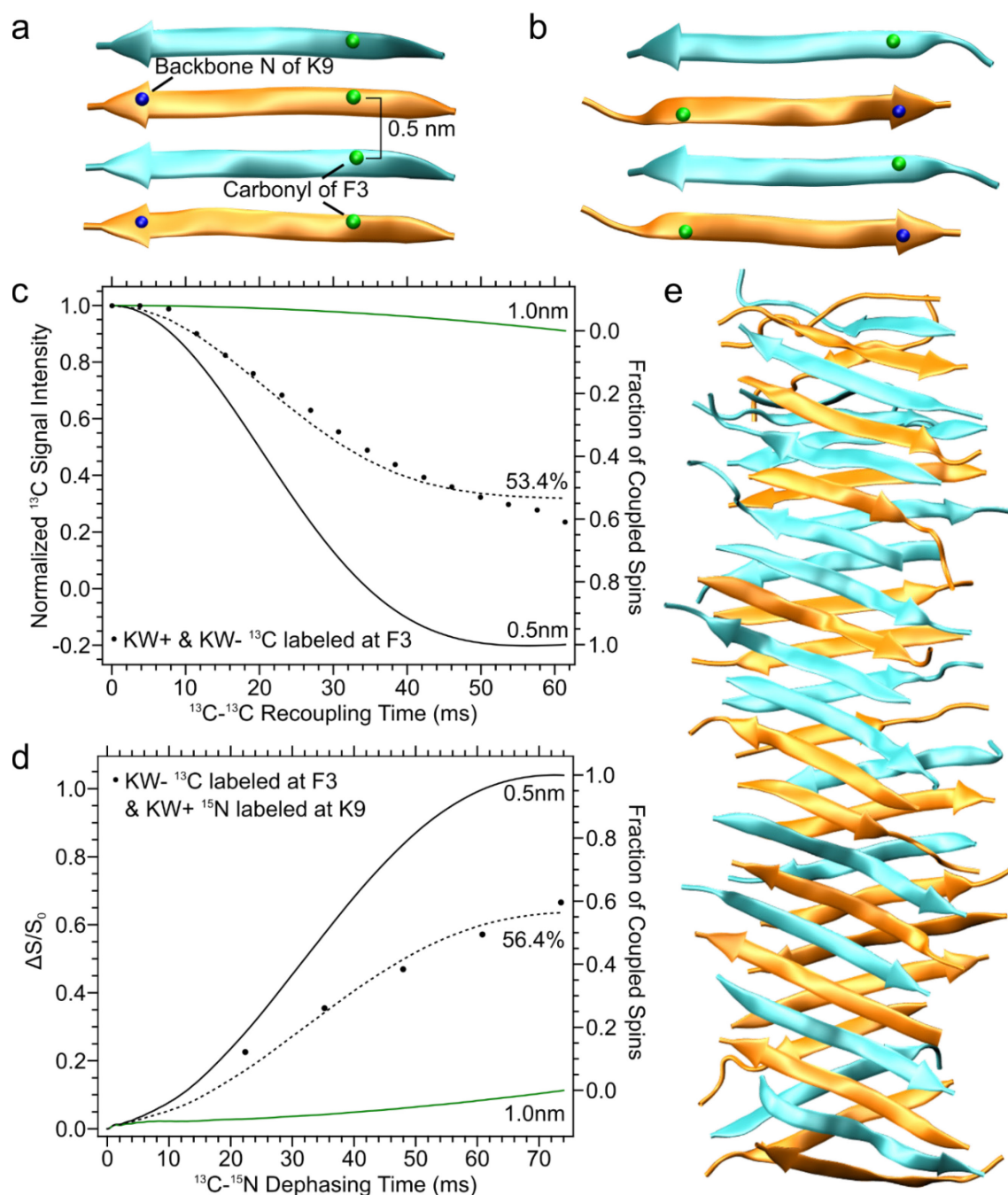


Figure 5. Dipolar recoupling experiments and coarse-grained DMD simulations of KW peptides show the presence of both parallel and antiparallel β -strands in co-assembled nanofibers. a) Illustration of the Sample E labeling scheme in a parallel β -sheet configuration. b) Illustration of the Sample E ($[1-^{13}\text{C}]\text{F3}$ and $[^{15}\text{N}]\text{K9}$ of KW+ and $[1-^{13}\text{C}]\text{F3}$ of KW-) labeling scheme in an antiparallel β -sheet configuration. c) ^{13}C - ^{13}C PITHIRDS-CT curves of Sample E. Solid curves represent SPINEVOLUTION simulations of PITHIRDS-CT data from pairs of spins separated by the indicated distance. The dotted curves are a linear combination of the simulated curves corresponding to 1.0 and 0.5 nm ^{13}C - ^{13}C distances, with 53.4% weighting of the 0.5 nm curve. d) $^{13}\text{C}\{^{15}\text{N}\}$ REDOR spectra of Sample E. Solid curves represent calculated REDOR dephasing curves for pairs of atoms separated by the specified distance. The dotted curve represents a linear combination of the simulated REDOR curves using 56.4% weighting of the curves for 0.5 nm. e) Representation of a β -sheet nanofiber observed in the coarse-grained DMD simulation.

Peptide Self-Association Observed in King-Webb Co-assembled β -Sheets.

Ideal co-assembly produces a perfectly alternating $(\text{AB})_n$ pattern within each β -sheet, where A and B correspond to KW+ and KW- peptide β -strands, respectively. In such a configuration, the β -sheet would be stabilized only through hydrogen bonding between complementary peptide molecules. However, solid-

state NMR measurements and DMD simulations show evidence of peptide self-association within the co-assembled nanofiber. Specifically, self-association refers to AA or BB nearest-neighbor interactions within a β -sheet. To detect KW+ and KW- self-association, PITHIRDS-CT experiments were conducted on nanofiber samples prepared with the CO site of F3 ^{13}C -enriched on one but not both peptide components (Samples F and G). Co-assembly of labeled and unlabeled peptides results in "isotopic

dilution" and reduction of ^{13}C - ^{13}C dipolar couplings. For co-assembled nanofibers with ideal $(\text{AB})_n$ alternation within β -sheets, the ^{13}C -labeled sites would be separated by at least 1 nm (see Figure 5b). Consequently, we would expect little detectable PITHIRDS-CT decays from Samples F or G. In contrast, peptide self-association would result in considerably stronger ^{13}C - ^{13}C dipolar couplings and increased signal decay because nearest-neighbor ^{13}C spacing would decrease to 0.5 nm. In Figure 6a, an intermediate ^{13}C signal decay is observed over 61.44 ms of recoupling time for isotopically diluted samples in the PITHIRDS-CT experiment. Figure 6b shows a segment of co-assembled nanofiber from the DMD simulation with noticeable peptide self-association along the β -sheet. In Figure S6, we present the F3 CO to F3 CO interstrand distance distribution calculated for KW+ peptides from DMD simulations. This distribution reveals a small peak around 0.5 nm, indicating that some KW+ peptides are adjacent to other KW+ peptides in the β -sheets. Similarly, a peak near 0.5 nm is observed in the distribution for the KW- chains, indicating KW- are also found to self-associate in the peptide nanofiber. These predictions of KW- and KW+ self-association in the co-assembled peptides align with experimental results detecting measurable peptide

self-association in isotopically diluted nanofiber samples. These findings are consistent with the Thioflavin T fluorescence measurements of β -sheet self-assembly in Figure 1b. Our measurements show that, while complementary peptide interactions between KW+ and KW- are kinetically favored, the peptides do have self-association tendencies.

Discussion

In this work, we provide direct evidence for the molecular-level co-assembly of KW+ and KW- peptides into β -sheet rich nanofibers. Although previous CD and FT-IR measurements performed on King-Webb peptides indirectly indicated co-assembly,¹¹ neither technique is capable of probing for molecular-level interactions between the two peptides within assembled nanofibers. By combining computational simulations with solid-state NMR experiments, we have shown molecular-level co-assembly between KW+ and KW- peptides occurs. Even though individual peptides can self-assemble within days, co-assembly is kinetically favored as observed by ThT fluorescence measurements and DMD simulations. Preference for co-assembly results from the strong electrostatic attraction between the oppositely charged peptides. These results are consistent with previous studies of co-assembling β -sheet systems based on enantiomeric peptides and oppositely charged A β (16-22) variants.^{12, 19} Analysis of NMR chemical shift peak areas uniquely attributable to the KW+ and KW- peptides in a quantitative ^{13}C spectrum reveals a near stoichiometric ratio of the two components, emphasizing the role of complementary interactions. Electrostatic interactions are effective in promoting peptide co-assembly at the molecular level while discouraging self-assembly. From our knowledge-based PRIME20 force field,⁶⁴ we know that the E sidechain has a strong electrostatic repulsion (sidechain-sidechain interaction strength, $\epsilon_{EE} = 3.15$ kJ/mol) with other E sidechains. In contrast, the K sidechain, although positively charged, has a relatively weak repulsion ($\epsilon_{KK} = 0.91$ kJ/mol) with other K sidechains; this behavior results from its large hydrophobic aliphatic sidechain. The KW+ peptide may have stronger resistance against self-assembly than the KW- peptide due to the stronger electrostatic repulsion from the 3 E residues in the middle of the KW+ peptide. We note that self-sorting could occur at different assembly conditions and relative peptide ratios as shown by Webber et al. on DWDW and KWKW peptides.⁴⁶ Furthermore, the agreement between experimental results and computational predictions showcases the power of coarse-grained DMD simulations. Although simulations and experiments access different assembly timescales, it is interesting that there appears to be a basis for direct comparison of assembled structure.

Despite recent reports that peptide self-assemblies tend to be monomorphic, including recent work on RADA16-I and MAX1,^{29, 47} co-assembled King-Webb peptides seem to exhibit a fundamental lack of preference for a single structure. Coarse-grained discontinuous molecular dynamics simulations predicted assembly into both parallel and antiparallel β -sheets which were also observed experimentally by dipolar recoupling

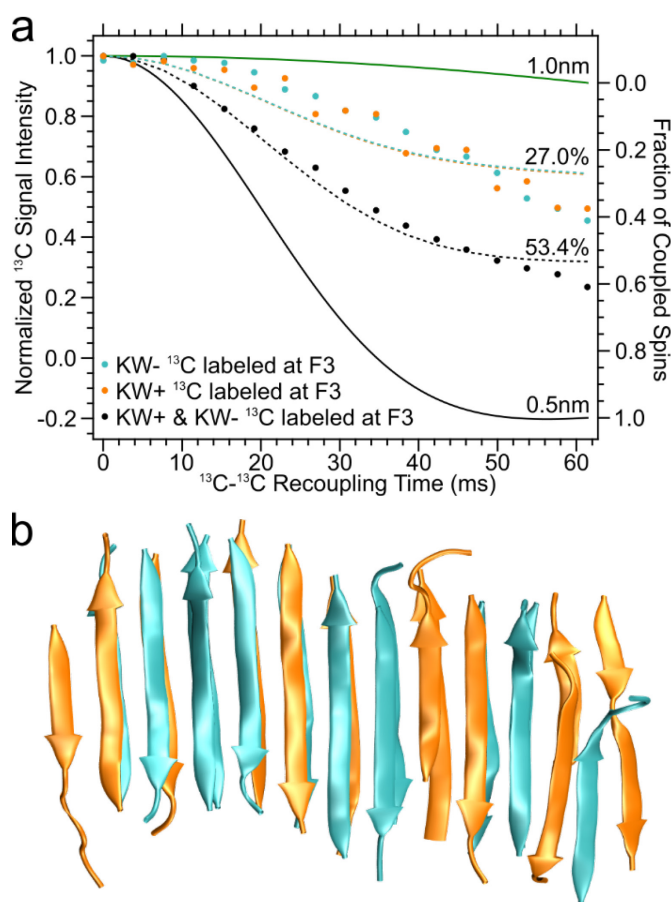


Figure 6. Self-association observed by NMR and coarse grained DMD simulations in co-assembled King-Webb peptide nanofibers. a) ^{13}C - ^{13}C PITHIRDS-CT decays measured for Sample F (orange) and Sample G (cyan). Solid curves represent SPINEVOLUTION simulations of 2-spin PITHIRDS-CT experiments. Dotted curves represent linear combinations using 1.0 and 0.5 nm simulations. b) Representation of a β -sheet nanofiber exhibiting peptide self-association as predicted in the coarse-grained DMD simulation.

NMR measurements. While the observation of antiparallel β -sheets matches the prediction from FT-IR spectra by King et al.,¹¹ our site-specific measurements showed an abundance of parallel β -sheets that would be unresolved by FT-IR. Estimation of the parallel and antiparallel β -sheet content from experimental results and computational predictions shows a preference for the expected antiparallel β -sheet structure (Table 2). Computational simulations show a mixture of β -strands aligned antiparallel and parallel along the same β -sheet, indicating that the addition of peptides in either orientation is favorable. Observation of this predicted behavior would be difficult to resolve by solid-state NMR. In addition, structure predictions from computational simulations reveal antiparallel β -sheets with a registry shift of 2 amino acids. Nanofibers produced from β -strands with a registry shift have a reduced number of hydrogen bonds, produce flexible peptide ends, and are skewed from the fiber axis (Figure 5e). Though there is no direct experimental evidence for this structural feature, the presence of antiparallel β -sheets with a registry shift is consistent with the increased PITHIRDS-CT signal decay and REDOR dephasing observed at longer recoupling times. We note that the presence of multiple structures in a single sample is rather unique. Though many self-assembling peptides can be assembled into various structures, the resulting polymorphic peptides generally produce nanofibers of a single favored structure for a given set of assembly conditions.²⁶⁻²⁸ In contrast, King-Webb peptide nanofibers surprisingly exhibit a mixture of several structures for a single assembly condition. Fast assembly kinetics may play a role in this structural heterogeneity though further studies would be needed. By combining computational simulations and experimental techniques, we have produced a detailed structural analysis of a highly heterogeneous co-assembled peptide nanofiber that would be difficult to assess with a singular technique.

Remarkably, self-association of KW+ and KW- peptides occurs in the co-assembled nanofiber samples. ThT fluorescence measurements showed that co-assembly is kinetically favored over self-assembly, but self-assembly occurs over 72 hours consistent with the time scale that KW+ and KW- peptides can self-associate into β -sheets. Evidence of the peptide self-association tendency was observed in the co-assembled nanofibers with dipolar recoupling NMR measurements on samples isotopically enriched on one peptide component at a time (Figure 6). These results are consistent with prior observations on co-assembled nanotubes of A β (16-22) derivatives where NMR measurements indicated a mixture of self-associated and complementary peptide leaflets.¹⁹ Given the high ionic strength of the assembly buffer (10X PBS), charge screening may facilitate KW+ and KW- self-association. Several self-assembling peptides have been shown to form gels upon adjusting the solution's ionic strength.⁴⁸⁻⁵⁰ Notably, the positively-charged MAX1 peptide forms β -hairpins that further assemble into β -sheet nanofibers in aqueous solution.²⁹ Also, P₁₁-4 and P₁₁-5 peptides, predecessors of the King-Webb peptides, exhibit a strongly pH-dependent self-assembly mechanism.¹⁴ In context, it is not surprising that counterions modulate effective interactions between like-charged

sidechains. Again, computational predictions are able to capture this non-ideal assembly behavior, providing an accurate view into the structural possibilities within co-assembled peptide nanofibers.

While charge complementarity produces peptides that exhibit co-assembly behavior, the King-Webb design does not produce well-controlled co-assembled nanofiber structures. Long-range electrostatic interactions in charge-complementary peptide systems may reduce the energy difference in parallel and antiparallel β -sheet structures allowing peptides in either orientation to add to the fiber end. Electrostatic forces may also affect the assembly pathway of charge-complementary peptides. Hydrogen bonding and hydrophobic interactions drive β -sheet formation in self-assembling peptides and contributions from charged residues can cause assembly to proceed along a different pathway dominated by charge complementarity.^{28,46} Coexistence of multiple peptide arrangements within the co-assembled nanofiber alludes to the possibility that peptides similar to the King-Webb peptides as long as favorable electrostatic interactions are formed. These peptides could belong to a family of co-assembling peptides capable of co-assembling with oppositely charged partners in a non-selective manner. While this lack of a strong preference for a specific arrangement may be desirable, we suggest that design of co-assembling peptides for more specific structures would aid in understanding the principles of creating co-assembled nanofibers.

Conclusions

The peptides introduced by from King et al. represent a successful design of a primarily co-assembled peptide nanofiber. Molecular level co-assembly was evaluated with computational simulations, biophysical measurements, and solid-state NMR spectroscopy. While charge-complementarity and the employed sidechain patterning do confer co-assembly over self-assembly, analysis of the molecular-level structure reveals a lack of precise control over local intermolecular organization. This level of structural precision may be sufficient for certain biotechnological applications such as a cell-culture scaffold, but as we seek to increase our ability to manipulate biological systems with synthetic materials, higher molecular-level precision may be desired. Next-generation designs will need to turn towards hydrophobic interactions, lock-and-key mechanisms, and sidechain complementarity to introduce structural specificity as seen in many self-assembling peptide systems and folded proteins.^{28, 42} Coarse-grained simulations may enable researchers to rapidly iterate through possible designs to identify well-controlled and highly selective co-assembling peptide designs similar to the computational work by Baker et al. to produce orthogonal coiled-coil oligomers.^{51, 52} Simulations can be combined with solid-state NMR techniques to reveal highly-resolved structural details to verify and validate new co-assembling peptide designs as shown in this study. Structural insights from these combined studies refine our understanding of sequence to structure relationships necessary in the design process. The ability to exhibit fine control over

peptide nanostructure will propel the design of supramolecular biomaterials beyond the designs in nature.

Materials and Methods

Unlabeled KW+ and KW- peptides were purchased from CPC Scientific, Inc. (Sunnyvale, CA). Labeled peptides were also purchased from CPC Scientific, Inc. synthesized using uniformly or partially ^{13}C and/or ^{15}N enriched amino acids supplied by Cambridge Isotope Laboratories, Inc.

Standard Hydrogel Preparation

All hydrogel samples were prepared by initially dissolving KW+ and KW- peptides in 10X PBS to produce 10mM solutions of single peptides. Equimolar mixtures of the KW+ and KW- peptide solutions were vortexed for 1 min and allowed to assemble. Initial assembly occurred within a few minutes, but samples were allowed to mature overnight for all samples. Isotopically labeled peptide samples were prepared according to labeling schemes in Table 1. Samples were centrifuged at 17.0 x g for 5 min. Supernatant was removed and fresh DI water added before resuspension. This wash cycle was repeated 2 more times. Solutions were flash-frozen in liquid nitrogen before lyophilization overnight.

Solid-State NMR Measurements

Lyophilized King-Webb peptide nanofibers were packed into Bruker 3.2 mm NMR rotors and 1 mg of water/mg of peptide was added to minimally hydrate the samples. All measurements except for REDOR experiments were performed on an 11.75 T Bruker Avance III spectrometer with a 3.2 mm Bruker MAS probe. ^1H - ^{13}C CPMAS measurements were run at 20 kHz magic angle spinning (MAS) with 100 kHz proton decoupling and a cross-polarization (CP) contact time set to 2 ms. NMR chemical shifts are referenced to tetramethyl silane, as calibrated using adamantane before each experiment. Quantitative ^1H - ^{13}C CPMAS measurements were run at 22 kHz magic angle spinning (MAS) and 100 kHz proton decoupling.³⁵ King-Webb nanofiber samples were run with 14 100 μs CP periods to ensure equivalent cross-polarization.

Finite-pulse Radio-Frequency Driven Recoupling (fpRFDR) and dipolar assisted rotational resonance (DARR) measurements were performed at a sample-rotation rate of 22 kHz to produce 2D ^{13}C - ^{13}C spectra. The mixing period for 2D DARR experiments was set to 500ms. 2D ^{13}C - ^{15}N TEDOR measurements were conducted with mixing times of 2.4 ms and 8 ms.

PITHIRDS-CT measurements were done at 12.5 kHz MAS with 26.7 μs π -pulses during ^{13}C dipolar recoupling. Total recoupling time was 61.44 ms, where $k_1 = 4$ and $k_2 + k_3 = 16.43$. Continuous wave proton decoupling at 100 kHz was applied during the PITHIRDS-CT pulse sequence and data acquisition, respectively. Sensitivity of PITHIRDS-CT measurements were improved by using pulsed spin locking.⁵³

REDOR measurements were performed using a 14.1 T Bruker Avance spectrometer with a 4 mm Bruker HXY MAS

probe. Pulse imperfections were compensated using xy8 phase cycling⁵⁴ of $^{15}\text{N}\{^{13}\text{C}\}$ REDOR 6 and 10 μs rotor-synchronized ^{13}C and ^{15}N π pulses, respectively. EXORCYCLE phase cycling^{55, 56} of the final ^{13}C Hahn-echo refocusing pulse was applied with 95 kHz Spinal64⁵⁷ ^1H decoupling as well. Active control of the MAS frequency was maintained at 10 kHz + 2 Hz. To ensure MAS and RF heating did not denature the samples, the cooling and spinning air exit temperature was maintained below -1 $^\circ\text{C}$. ^{13}C (150.8 MHz) and ^{15}N (60.8 MHz) CPMAS spectra before and after REDOR experiments sample integrity during the experiment. The sum of center and sideband peak heights is used to calculate REDOR data points.

Dipolar Recoupling Spin Simulations

Calculation of signal decay curves from PITHIRDS-CT experiments were produced by using SpinEvolution NMR simulation software.⁵⁸ Simulations were run with 2 nuclear spins set at 5.0 \AA or 10.0 \AA distances. Attenuated decay was quantified using linear combinations of simulated PITHIRDS-CT decay curves at 5.0 \AA and 10.0 \AA to fit experimental spectra.

A single ^{15}N spin in the presence of one ^{13}C spin spaced 0.5 or 1.0 nm apart were simulated for REDOR analysis.⁴⁵ Contributions from naturally abundant carbonyl carbons and ^{15}N desphasing from these carbons were included.⁵⁹

Transmission Electron Microscopy (TEM)

Co-assembled KW+ and KW- nanofibers were deposited onto 400 mesh lacey carbon-coated Cu electron microscopy grids (TED Pella, INC.) and strained with 1 wt% uranyl acetate. TEM images were taken using a Hitachi HT-7700 electron microscope at an accelerating voltage of 80 keV.

Thioflavin T (ThT) Analysis

A stock solution containing 0.8 mg/mL of thioflavin T (ThT) (Acros) in water was filtered through a 0.22 μm syringe filter (Millex). Peptides in water, ThT, and PBS were added to a black 96-well plate (Corning) to obtain a final concentration of 500 μM total peptide, 0.08 mg/mL ThT, and 10x PBS. Samples were analyzed with a Molecular Devices SpectraMax M3 spectrophotometer (excitation 450 nm, emission 482 nm). All samples were run in triplicate, with the mean and standard deviation of these samples reported.

All-Atom Models of Ideal β -Sheet Structures

Idealized all-atom models of 4 possible β -sheet nanofiber structures were built to aid interpretation of intermolecular contacts observed by solid-state NMR. All β -sheet models were constructed using NAMD molecular dynamics and VMD software.⁶⁰⁻⁶² Initial models of the KW+ and KW- peptides were individually created in VMD with the molefactory plugin. KW+ and KW- monomers were manipulated depending on the β -sheet structure and stacking and repeated along the fiber axis using Mathematica to produce a 2 β -sheets with 10 units each (5 KW+ and 5 KW-) which were stacked to form a hydrophobic core. Using NAMD molecular dynamics software, artificial

dihedral angle and hydrogen bond constraints were introduced and the constrained structure was energy minimized for 10 ps in implicit solvent. Then, the temperature was increased from 0 K to 500 K followed by cooling to 300 K in 10 K increments with 10 ps simulation time per step in implicit solvent. Following a 25 ps equilibration period, the two β -sheets were stacked into a 2-layer nanofiber by artificially constraining intersheet distances. The constrained bilayer nanofiber structure was energy minimized for 10 ps, heated from 0 to 300 K in 10 K per 10 ps increments before a final equilibration period of 20 ps. Visualization of the co-assembled KW+ and KW- peptide nanofibers was done with VMD (Visual Molecular Dynamics) software. Analysis of intermolecular contacts and distances for comparison with solid-state NMR measurements were performed using custom code in Wolfram Mathematica.

Coarse Grained Discontinuous Molecular Dynamics Simulations

Our simulation method is discontinuous molecular dynamics (DMD), a fast alternative to traditional molecular dynamics.⁶³ It is used in conjunction with PRIME20, an implicit-solvent coarse-grained protein force field developed in the Hall group that is tailored to simulate peptide aggregation.⁶⁴⁻⁶⁶ In the PRIME20 model, each of 20 residue contains three backbone spheres NH, C α , CO and one sidechain sphere R with a unique set of geometric parameters: a hard sphere diameter (effective van der Waals radius), sidechain-to-backbone distances (R-C α , R-NH, R-CO) for each sidechain. The potential function between two residue sidechain spheres is modeled as a square well potential. The parameter matrix between any two of twenty different sidechain-sidechain interactions include 210 different square well widths and 19 different square well depths to discriminate the polar, charge-charge and hydrophobic types of interactions.⁶⁴ The hydrogen bonding interaction between backbone beads NH and CO is modeled as a directional square well potential. All the other non-bonded interactions are modeled as hard sphere potentials. A detailed description of the geometric and energetic parameters of the PRIME20 model is provided in our earlier work.^{64, 67, 68}

In this work, we performed large-scale DMD/PRIME20 simulations to evaluate the spontaneous aggregation propensities and co-assembled structures of King-Webb peptides. All of the simulations are carried out for 30-36 μ s in the canonical (NVT) ensemble at a peptide concentration of 20 mM. The Andersen thermostat is implemented to maintain the simulation system at a constant temperature.⁶⁹ For the peptide co-assembly cases, 48 A and 48 B peptides are initially randomly placed in a cubic box with a length of 200.0 Å, corresponding to a peptide concentration of 20 mM. The reduced temperature is defined to be $T^* = kBT/\epsilon_{HB}$, where $\epsilon_{HB} = 12.47$ kJ/mol is the hydrogen bonding energy. We set the reduced temperature T^* of the simulations to be 0.19, which corresponds to 319 K in real temperature unit.⁶⁷ For the peptide self-assembly cases, single peptide species system containing either 48 A or 48 B are kept at the same concentration as in the co-assembly cases by reducing the cubic simulation box length to 159.0 Å. The simulation temperature is also kept the same as in the co-

assembled King-Webb simulations. We repeat the simulation three times for each of the systems mentioned above. Simulations are run at the previously specified temperature and concentration to reduce aggregation lag phases and nucleation barriers.

Conflicts of interest

There are no conflicts to declare.

Acknowledgements

This research was supported by funds from the National Science Foundation Grant CBET-1743432. The authors acknowledge the use of instruments in the NMR Center at the Georgia Institute of Technology and the Robert P. Apkarian Integrated Microscopy Core at Emory University.

Notes and references

- 1 E. Busseron, Y. Ruff, E. Moulin and N. Giuseppone, *Nanoscale*, 2013, **5**, 7098-7140.
- 2 E. C. Wu, S. Zhang and C. A. E. Hauser, *Adv. Funct. Mater.*, 2012, **22**, 456-468.
- 3 J. P. Jung, A. K. Nagaraj, E. K. Fox, J. S. Rudra, J. M. Devgun and J. H. Collier, *Biomaterials*, 2009, **30**, 2400-2410.
- 4 M. M. Ouberai, A. L. G. Dos Santos, S. Kinna, S. Madalli, D. C. Hornigold, D. Baker, J. Naylor, L. Sheldrake, D. J. Corkill, J. Hood, P. Vicini, S. Uddin, S. Bishop, P. G. Varley and M. E. Welland, *Nature Communications*, 2017, **8**, 1026.
- 5 S. Eskandari, T. Guerin, I. Toth and R. J. Stephenson, *Adv. Drug Del. Rev.*, 2017, **110-111**, 169-187.
- 6 L. H. Tostanoski and C. M. Jewell, *Adv. Drug Del. Rev.*, 2017, **114**, 60-78.
- 7 J. S. Rudra, T. Sun, K. C. Bird, M. D. Daniels, J. Z. Gasiorowski, A. S. Chong and J. H. Collier, *ACS Nano*, 2012, **6**, 1557-1564.
- 8 J. S. Rudra, Y. F. Tian, J. P. Jung and J. H. Collier, *Proceedings of the National Academy of Sciences*, 2010, **107**, 622-627.
- 9 N. L. Truex, Y. Wang and J. S. Nowick, *J. Am. Chem. Soc.*, 2016, **138**, 13882-13890.
- 10 D. T. Seroski, A. Restuccia, A. D. Sorrentino, K. R. Knox, S. J. Hagen and G. A. Hudalla, *Cell. Mol. Bioeng.*, 2016, **9**, 335-350.
- 11 P. J. King, M. Giovanna Lizio, A. Booth, R. F. Collins, J. E. Gough, A. F. Miller and S. J. Webb, *Soft Matter*, 2016, **12**, 1915-1923.
- 12 R. J. Swanekamp, J. T. M. DiMaio, C. J. Bowerman and B. L. Nilsson, *J. Am. Chem. Soc.*, 2012, **134**, 5556-5559.
- 13 S. Kyle, S. H. Felton, M. J. McPherson, A. Aggeli and E. Ingham, *Advanced Healthcare Materials*, 2012, **1**, 640-645.
- 14 A. Aggeli, M. Bell, L. M. Carrick, C. W. G. Fishwick, R. Harding, P. J. Mawer, S. E. Radford, A. E. Strong and N. Boden, *J. Am. Chem. Soc.*, 2003, **125**, 9619-9628.
- 15 M. Varadi, G. De Baets, W. F. Vranken, P. Tompa and R. Pancsa, *Nucleic Acids Res.*, 2017, **46**, D387-D392.
- 16 S.-Y. Fung, H. Yang, P. Sadatmousavi, Y. Sheng, T. Mamo, R. Nazarian and P. Chen, *Adv. Funct. Mater.*, 2011, **21**, 2456-2464.
- 17 M. Belli, M. Ramazzotti and F. Chiti, *EMBO reports*, 2011, **12**, 657-663.
- 18 R. V. Uljijn and A. M. Smith, *Chem. Soc. Rev.*, 2008, **37**, 664-675.
- 19 S. Li, A. K. Mehta, A. N. Sidorov, T. M. Orlando, Z. Jiang, N. R. Anthony and D. G. Lynn, *J. Am. Chem. Soc.*, 2016, **138**, 3579-3586.

- 20 M. J. Pandya, G. M. Spooner, M. Sunde, J. R. Thorpe, A. Rodger and D. N. Woolfson, *Biochemistry*, 2000, **39**, 8728-8734.
- 21 A. Aggeli, M. Bell, N. Boden, J. N. Keen, P. F. Knowles, T. C. B. McLeish, M. Pitkeathly and S. E. Radford, *Nature*, 1997, **386**, 259-262.
- 22 J. H. Collier and P. B. Messersmith, *Bioconj. Chem.*, 2003, **14**, 748-755.
- 23 G. Zandomenighi, M. R. H. Krebs, M. G. McCammon and M. Fändrich, *Protein Sci.*, 2004, **13**, 3314-3321.
- 24 A. R. Cormier, X. Pang, M. I. Zimmerman, H. X. Zhou and A. K. Paravastu, *ACS Nano*, 2013, **7**, 7562-7572.
- 25 H. Yokoi, T. Kinoshita and S. Zhang, *Proc. Natl. Acad. Sci. U.S.A.*, 2005, **102**, 8414-8419.
- 26 B. H. Meier, R. Riek and A. Böckmann, *Trends Biochem. Sci.*, 2017, **42**, 777-787.
- 27 R. Kodali, A. D. Williams, S. Chemuru and R. Wetzel, *J. Mol. Biol.*, 2010, **401**, 503-517.
- 28 J. Park, B. Kahng and W. Hwang, *PLoS Comp. Biol.*, 2009, **5**, e1000492-e1000492.
- 29 K. Nagy-Smith, E. Moore, J. Schneider and R. Tycko, *Proceedings of the National Academy of Sciences*, 2015, **112**, 9816-9821.
- 30 H. Naiki, K. Higuchi, M. Hosokawa and T. Takeda, *Anal. Biochem.*, 1989, **177**, 244-249.
- 31 M. Biancalana and S. Koide, *Biochim. Biophys. Acta*, 2010, **1804**, 1405-1412.
- 32 K. Takegoshi, S. Nakamura and T. Terao, *Chem. Phys. Lett.*, 2001, **344**, 631-637.
- 33 Y. Ishii, *The Journal of Chemical Physics*, 2001, **114**, 8473-8483.
- 34 A. E. Bennett, C. M. Rienstra, J. M. Griffiths, W. Zhen, P. T. L. Jr. and R. G. Griffin, *The Journal of Chemical Physics*, 1998, **108**, 9463-9479.
- 35 P. Duan and K. Schmidt-Rohr, *J. Magn. Reson.*, 2017, **285**, 68-78.
- 36 D. S. Wishart, *Prog Nucl Mag Res Sp*, 2011, **58**, 62-87.
- 37 E. L. Ulrich, H. Akutsu, J. F. Doreleijers, Y. Harano, Y. E. Ioannidis, J. Lin, M. Livny, S. Mading, D. Maziuk, Z. Miller, E. Nakatani, C. F. Schulte, D. E. Tolmie, R. K. Wenger, H. Y. Yao and J. L. Markley, *Nucleic Acids Res.*, 2008, **36**, D402-D408.
- 38 D. Wishart and B. Sykes, *J. Biomol. NMR*, 1994, **4**, 171-180.
- 39 J. R. Lewandowski, P. C. A. van der Wel, M. Rigney, N. Grigorieff and R. G. Griffin, *J. Am. Chem. Soc.*, 2011, **133**, 14686-14698.
- 40 C. P. Jaroniec, C. Filip and R. G. Griffin, *J. Am. Chem. Soc.*, 2002, **124**, 10728-10742.
- 41 S. G. Zech, A. J. Wand and A. E. McDermott, *J. Am. Chem. Soc.*, 2005, **127**, 8618-8626.
- 42 M. R. Sawaya, S. Sambashivan, R. Nelson, M. I. Ivanova, S. A. Sievers, M. I. Apostol, M. J. Thompson, M. Balbirnie, J. J. W. Wiltzius, H. T. McFarlane, A. O. Madsen, C. Riek and D. Eisenberg, *Nature*, 2007, **447**, 453-457.
- 43 R. Tycko, *J. Chem. Phys.*, 2007, **126**, 064506-064506.
- 44 C. P. Jaroniec, B. A. Tounge, C. M. Rienstra, J. Herzfeld and R. G. Griffin, *J. Magn. Reson.*, 2000, **146**, 132-139.
- 45 J. M. Goetz and J. Schaefer, *J. Magn. Reson.*, 1997, **127**, 147-154.
- 46 J. K. Sahoo, M. A. VandenBerg, E. E. Ruiz Bello, C. D. Nazareth and M. J. Webber, *Nanoscale*, 2019, **11**, 16534-16543.
- 47 A. R. Cormier, X. Pang, M. I. Zimmerman, H.-X. Zhou and A. K. Paravastu, *ACS Nano*, 2013, **7**, 7562-7572.
- 48 M. R. Caplan, P. N. Moore, S. Zhang, R. D. Kamm and D. A. Lauffenburger, *Biomacromolecules*, 2000, **1**, 627-631.
- 49 L. M. Carrick, A. Aggeli, N. Boden, J. Fisher, E. Ingham and T. A. Waigh, *Tetrahedron*, 2007, **63**, 7457-7467.
- 50 F. Koch, M. Müller, F. König, N. Meyer, J. Gattlen, U. Piele, K. Peters, B. Kreikemeyer, S. Mathes and S. Saxer, *Royal Society open science*, 2018, **5**, 171562-171562.
- 51 Z. Chen, S. E. Boyken, M. Jia, F. Busch, D. Flores-Solis, M. J. Bick, P. Lu, Z. L. VanAernum, A. Sahasrabudde, R. A. Langan, S. Bermeo, T. J. Brunette, V. K. Mulligan, L. P. Carter, F. DiMaio, N. G. Sgourakis, V. H. Wysocki and D. Baker, *Nature*, 2019, **565**, 106-111.
- 52 S. E. Boyken, Z. Chen, B. Groves, R. A. Langan, G. Oberdorfer, A. Ford, J. M. Gilmore, C. Xu, F. DiMaio, J. H. Pereira, B. Sankaran, G. Seelig, P. H. Zwart and D. Baker, *Science*, 2016, **352**, 680-687.
- 53 A. T. Petkova and R. Tycko, *J. Magn. Reson.*, 2002, **155**, 293-299.
- 54 T. Gullion, D. B. Baker and M. S. Conradi, *Journal of Magnetic Resonance (1969)*, 1990, **89**, 479-484.
- 55 N. Sinha, K. Schmidt-Rohr and M. Hong, *J. Magn. Reson.*, 2004, **168**, 358-365.
- 56 M. Rance and R. A. Byrd, *Journal of Magnetic Resonance (1969)*, 1983, **52**, 221-240.
- 57 B. M. Fung, A. K. Khitrin and K. Ermolaev, *J. Magn. Reson.*, 2000, **142**, 97-101.
- 58 M. Veshkort and R. G. Griffin, *J. Magn. Reson.*, 2006, **178**, 248-282.
- 59 G. M. Bernard, M. Miskolzie, G. Kotovych and R. E. Wasylshen, *Can. J. Chem.*, 2004, **82**, 1554-1563.
- 60 J. C. Phillips, R. Braun, W. Wang, J. Gumbart, E. Tajkhorshid, E. Villa, C. Chipot, R. D. Skeel, L. Kalé and K. Schulten, *J. Comput. Chem.*, 2005, **26**, 1781-1802.
- 61 M. T. Nelson, W. Humphrey, A. Gursoy, A. Dalke, L. V. Kalé, R. D. Skeel and K. Schulten, *The International Journal of Supercomputer Applications and High Performance Computing*, 1996, **10**, 251-268.
- 62 W. Humphrey, A. Dalke and K. Schulten, *J. Mol. Graphics*, 1996, **14**, 33-38.
- 63 B. J. Alder and T. E. Wainwright, *The Journal of Chemical Physics*, 1959, **31**, 459-466.
- 64 M. Cheon, I. Chang and C. K. Hall, *Proteins: Structure, Function, and Bioinformatics*, 2010, **78**, 2950-2960.
- 65 Y. Wang, S. J. Bunce, S. E. Radford, A. J. Wilson, S. Auer and C. K. Hall, *Proceedings of the National Academy of Sciences*, 2019, **116**, 2091-2096.
- 66 S. J. Bunce, Y. Wang, K. L. Stewart, A. E. Ashcroft, S. E. Radford, C. K. Hall and A. J. Wilson, *Science advances*, 2019, **5**, eaav8216-eaav8216.
- 67 Y. Wang, Q. Shao and C. K. Hall, *J. Biol. Chem.*, 2016, **291**, 22093-22105.
- 68 H. D. Nguyen and C. K. Hall, *Proc. Natl. Acad. Sci. U.S.A.*, 2004, **101**, 16180-16185.
- 69 H. C. Andersen, *The Journal of Chemical Physics*, 1980, **72**, 2384-2393.